Asian Journal of Chemistry; Vol. 36, No. 12 (2024), 2891-2898

ASIAN JOURNAL OF CHEMISTRY

https://doi.org/10.14233/ajchem.2024.32780

AC Conductivity, Dielectric and Structural Properties of $Co_{0.6}Zn_{0.4-x}Mg_xFe_2O_4$ Co-Zn Spinel Nano Ferrites Prepared using Sol-gel Autocombustion Method

PUSHPA N. AWANTI[1,2], M.V. MURUGENDRAPPA[3], SHARANAPPA CHAPI[3], SHRIDHAR N. MATHAD[4], R.B. KONDA[5] and SHIVRAJ G. GOUNHALLI[2,*]

[1]Department of Physics, Government First Grade College, Patrakarta Nagar, Hubballi-580032, India
[2]Department of Physics, Smt. Veeramma Gangasiri College for Women, Kalaburagi-585102, India
[3]Department of Physics, B.M.S. College of Engineering, Bengaluru-560019, India
[4]Department of Engineering Physics, K.L.E. Institute of Technology, Hubballi-580030, India
[5]Department of Electronics, Smt. Veeramma Gangasiri College for Women, Kalaburagi-585102, India

*Corresponding author: E-mail: sgg19777@gmail.com

Received: 26 September 2024; *Accepted*: 7 November 2024; *Published online*: 30 November 2024; AJC-21832

This study examined the structural, morphological, dielectric and AC conductivity properties of CoZnMg ferrite samples ($Co_{0.6}Zn_{0.4-x}Mg_xFe_2O_4$) with x = 0.00, 0.08, 0.16, 0.24, 0.32, 0.40. The sol-gel autocombustion method was used to synthesize the CoZnMg ferrite samples. The produced samples crystallize in the cubic spinel structure, according to an XRD analysis of the structural characteristics. The highly crystalline single-phase cubic spinel structure with a distinct peak in the (311) plane has been confirmed by XRD studies. The diameters of the crystallites have fluctuated between 24.92 and 9.80 nm. SEM, EDX and FTIR used to examine the morphological and elemental characteristics of the samples. According to FE-SEM, adding magnesium to the current ferrite system resulted in the loss of the porous gel structure. According to the relative stoichiometry of the Mg-substituted CoZn ferrite, the EDAX analysis verified the presence of Co, Zn, Mg and O. The investigated samples may be appropriate for a variety of uses, as indicated by the consistent conductivity at low frequencies. Within the frequency range of 100 to 5 MHz, the room temperature, electrical and dielectric properties were examined. The quantity of magnesium dopants and the microstructural features were related to the obtained results. The dielectric characteristics (ε′ and ε″) of the ferrites gradually decreased with frequency, even at higher frequencies. The samples exhibited interfacial polarization, which led to normal dielectric characteristics in line with the Maxwell-Wagner model.

Keywords: CoZn ferrite, Sol-gel method, Dielectric properties, AC conductivity, Maxwell-Wagner model.

INTRODUCTION

Materials have remarkable responses at the nanoscale, exhibiting improved chemical and physical characteristics. The principles of physics offered a more foundational understanding of this patentable trait, however a decrease in the disparity of characteristics aligns with nature's new principle [1]. As a result, nanomaterials are the subject of nanotechnology because of their unique applications resulting from their nanosized size [2]. Ferrites are hard and brittle, similar to the majority of ceramics. The superexchange interaction between metal electrons and oxygen ions causes ferrimagnetism in ferrites. Because of the opposite spins, ferrite is less magnetic than ferromagnetic metals with parallel spins. Ferrite is more resistive than ferromagnetic metals due to the inherent atomic-level interaction between metal ions and oxygen [3-5]. This has enormous technological significance, since it makes ferrite usable at higher frequencies.

In general, ferrites can be divided into four major types based on their composition and structure *viz.* garnet, spinel, hexagonal and perovskite-type ferrites [6-9]. Spinel ferrites are an important class of oxide materials with the general formula AFe_2O_4, where A can be any metal ion. The distribution of cations in interstates determines the magnetic and electrical properties of materials [10-13]. The characteristics of spinel ferrites depend on a number of variables, including the synthesis technique used, time and temperature, stoichiometric ratio, cationic distributions at the tetrahedral and octahedral sites, particle size and shape [14].

The sol-gel method, in particular, is a productive technology that may be utilized to regulate the microstructure, grain size and flaw distribution of materials [15]. Magnesium spinel ferrites composites exhibit significant chemical stability, large magnetic anisotropy, moderate saturation magnetization, good chemical stability and good mechanical toughness [16]. Multicomponent nanoparticles produced by this process are homogenous and non-agglomerated. The combination of a reducing agent (fuel) with an oxidizing agent (metal nitrates) is the basis of this process. As it determines the morphology, grain size and crystal structure, the latter is crucial. Compared to physical and chemical synthesis techniques, green synthesis technologies provide a straightforward and effective substitute.

According to Chahar *et al.* [17], the production of Ni-doped Co-Zn nanoferrite particles was accomplished using a citrate precursor method. The single-phase spinel cubic symmetry of ferrite nanoparticles was shown by XRD and exhibit good dielectric characteristics; for various Ni-doped samples, values of ε′ and ε″ range from 3.06 to 13.77 and 0.23-3.6, respectively. The spinel ferrites ZMCCF: $Zn_{0.5-x}Mg_{0.25} + xCo_{0.25}Cr_{1-x}Fe_{1+x}O_4$ offer remarkable structural, morphological and dielectric properties, according to Hasanain [18]. According to Koop's theory, the spinel ferrites exhibit a beneficial trend whereby their dielectric constant drops as frequency increases. Similarly, the synthesis of $Ni_{0.4}M_{0.2}Zn_{0.4}Fe_2O_4$ (M = Ni^{2+}, Mg^{2+} and Co^{2+}) nanoparticles was carried out by Hasan & Azdhar [19] using the sol-gel auto-combustion approach. It was observed that the AC conductivity of the nanoparticles decreased when Mg^{2+} and Co^{2+} were substituted into Ni–Zn ferrite.

Following an extensive review of the literature on this compound, it is observed that there has not been a precise and comprehensive investigation of the physical properties (structural, morphological, electric and dielectric) of this compound when magnesium was substituted. For the $Co_{0.6}Zn_{0.4-x}Mg_xFe_2O_4$, ferrite system, the dielectric behaviour and AC electrical conductivity were examined at room temperature. The dielectric behaviour of $Co_{0.6}Zn_{0.4-x}Mg_xFe_2O_4$ ferrites has seldom been discussed in the literature. Therefore, this study aims to systematically examine the effects of magnesium substitution on the physical properties and applications of spinel ferrites in energy storage, photocatalysis and microelectronics. The findings show that this compound possesses exceptional electrical and dielectric qualities, such as low conductivity, high permittivity at room temperature and low frequencies, which makes it very appealing for the creation of microwave and electrical devices. For the $Co_{0.6}Zn_{0.4-x}Mg_xFe_2O_4$ ferrite sample, the dielectric behaviour, AC electrical conductivity and scanning electron microscopy were carried out.

EXPERIMENTAL

AR-grade nitrate cobalt nitrate hexahydrate [$Co(NO_3)_2 \cdot 6H_2O$], nickel nitrate hexahydrate [$Ni(NO_3)_2 \cdot 6H_2O$], copper nitrate hexahydrate [$Mg(NO_3)_2 \cdot 6H_2O$], zinc nitrate tetrahydrate [$Zn(NO_3)_2 \cdot 4H_2O$), ferric nitrate nonahydrate ($Fe(NO_3)_3 \cdot 9H_2O$) and urea were acquired from LOBA CHEMIE Pvt. Ltd. and used exactly as supplied.

Synthesis: The starting precursors (Co, Ni, Zn, Fe and Mg) were dissolved in deionized water to prepare an aqueous solution with a stoichiometric ratio. After the pure solution formed, the water started to evaporate on a heated plate forming a dry, thick gel. Further heating caused a self-propagating combustion event to occur in the gel at a certain point, which was followed by a dense evolution of brown gases, primarily nitrogen oxides. The flame spread until the entire gel turned into a powder that appeared burned fluffy ash. After that, the coarse powder was collected and finely ground in an agate mortar to produce a fine powder. To remove volatile materials from the material being processed, such as water, carbon dioxide or organic compounds, the sample was further calcined at 800 ºC for 3 h.

In the next step, to obtain Mg^{2+} substituted Co and Zn ferrites, the powder was then formed into pellets with a diameter of 10 mm and a thickness of nearly 2 mm using a manual pressing machine with a pressure of 10 tons. To produce a parallel plate capacitor shape with ferrite acting as dielectric medium, the surfaces of the pellets were polished and coated with silver paste. The developed ferrites have a general composition of $Co_{0.6}Zn_{0.4-x}Mg_xFe_2O_4$ (where x = 0, 0.08, 0.16, 0.24, 0.32 and 0.40).

Characterization: Using a Philips model (PW-1729) diffractometer (Cu-$K\alpha$ radiation source with λ = 1.540598 Å) with 2θ in the range of 10º to 80º, the samples were analyzed by X-ray diffraction. Using a Perkin-Elmer-1430, FTIR spectra were recorded for the prepared samples at room temperature in the 4000–400 cm^{-1} range. The field emission scanning electron microscopy (FESEM) was used to examine the microstructure of the samples. The impedance of each pallet sample was measured at room temperature for a different frequency using a Wayne Kerr 6500B precision impedance analyzer at different temperatures the electrical and dielectric properties were measured from 20 Hz to 1 MHz [20].

RESULTS AND DISCUSSION

XRD studies: Fig. 1 displays the X-ray diffraction (XRD) patterns of all synthesized samples in the 2θ range of 20-80º. The standard pattern indices of all of the major peaks, which are found to be the (2 2 0), (3 1 1), (4 0 0), (4 4 2), (5 1 1) and (4 4 0) planes indicate that their structure was single-phase. When the concentration of Mg increased, the lattice constant and unit cell volume of the samples decreased. Ultrafine particles in the samples are responsible for the widening and low intensity of the diffraction peaks. Using the following relations, the structural and microstructural parameters were computed. Using Bragg's diffraction conditions and the 2θ values of the most intense peaks, the average lattice constant values (a) were determined [21].

$$a = \frac{\lambda\sqrt{h^2 + k^2 + l^2}}{2\sin\theta} \quad (1)$$

The Debye-Sherrer's equation (eqn. 2) [22] is used to compute the average crystallite sizes with the full width at half maximum of the most intense peaks.

$$D = \frac{k\lambda}{\beta\cos\theta} \quad (2)$$

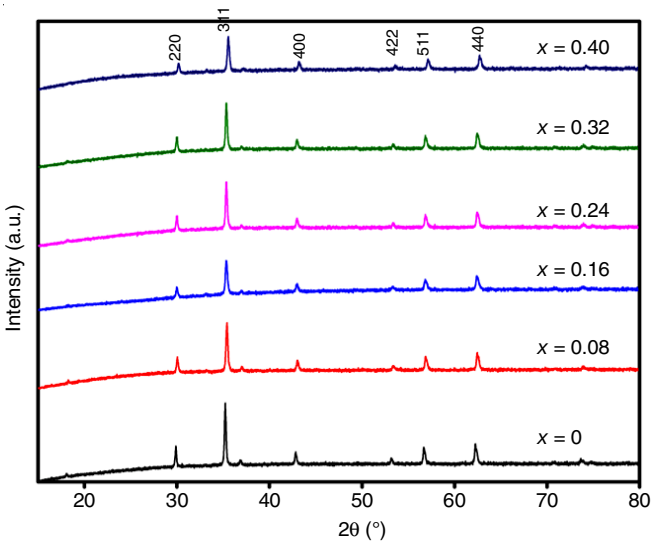

Fig. 1. XRD spectra of Mg^{2+} doped nanoferrites

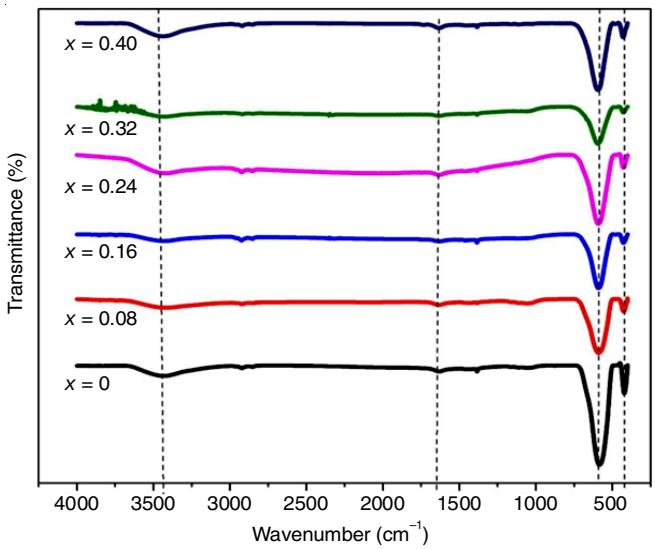

Fig. 2. FTIR spectra of Mg^{2+} doped nanoferrites

where λ is the X-ray wavelength; β is the full width at half maximum intensity accounting for instrumental broadening, and K is the form factor, which is chosen to be 0.89.

Furthermore, as the crystalline size decreases, the volume of a cell is computed using eqn. 4. Similarly, the characteristics of $Co_{0.6}Zn_{0.4-x}Mg_xFe_2O_4$ nanoparticles are determined by their cationic distribution and lattice strain. Here, the uniform strains are assumed in all crystallographic directions, which are established by eqn. 3. By the use of a relay, the strain and dislocation density produced in the nanocrystals are computed.

$$\varepsilon = \frac{\beta}{4\tan\theta} \tag{3}$$

$$\delta = \frac{1}{D^2} \tag{4}$$

Lattice constant values known as hopping lengths at the tetrahedral (A) and octahedral (B) sites were used to calculate the distance between the magnetic ions in all the samples.

$$L_A = a \times \frac{\sqrt{3}}{4} \tag{5}$$

$$L_B = a \times \frac{\sqrt{2}}{4} \tag{6}$$

The results of the all the parameters are tabulated in Table-1.

FTIR studies: Fig. 2 displays the FTIR spectra of the nanocrystal powders in the 4000-400 cm^{-1} range. The metal oxygen (M-O) vibration mode bands below 1000 cm^{-1} are common in ferro spinel ferrites spectra. These spectra show the distinctive qualities of spinel ferrites. The high-frequency band was found to be in the 583-416 cm^{-1} region. The absence of any further group peaks indicated that the synthetic material used to create the fingerprint was devoid of organic chemicals.

The metal oxygen stretching frequencies are attributed to the absorption bands. In comparison to the M-O stretching frequency of octahedral (O_h-M-O) sites, the observed stretching frequency is expected to increase [22]. Waldron suggested that the octahedral and tetrahedral sites of the cubic spinel unit cell can be used to create vibrations. A minor change in the band's frequency towards the higher frequency side is observed in the band position.

SEM studies: Fig. 3a-c shows FESEM images of the spinel $Co_{0.6}Zn_{0.4-x}Mg_xFe_2O_4$ (where $x = 0, 0.08, 0.16, 0.24, 0.32, 0.40$) samples. The approximately symmetrical and packed grains were observed. The replacement of Mg^{2+} ions had an impact on the size and shape of the particles. The size of the molecule changes due to the significant increase in Mg^{2+} ions; it grows from 30 to 35 nm. Grain growth is inhibited by the presence of Mg on the grain border.

Energy dispersive X-ray analysis is a technique utilized to qualitatively and quantitatively analyze the composition of $Co_{0.6}Zn_{0.4-x}Mg_xFe_2O_4$ (x = 0, 0.08, 0.16, 0.24, 0.32 and 0.40) samples both. The acquired EDX patterns are displayed in Fig. 4. The stoichiometric analysis of the sample composition derived from the EDS analysis revealed the presence of Co,

TABLE-1
EXPERIMENTALLY DETERMINED PARAMETERS OF VARIOUS Mg^{2+} DOPED NANOFERRITES

Composition	Crystallite size, D (nm)	Interplanar spacing, d (Å)	Lattice parameter, a (Å)	Strain, $\varepsilon \times 10^{-3}$	Dislocation density, $\delta \times 10^{14}$ m^{-2}	L_A (Å)	L_B (Å)
0	27.13	2.5447	0.7673	4.14	3.6	0.664501	0.271282
0.08	22.53	2.5428	0.7667	5.00	5.7	0.663982	0.271069
0.16	18.51	2.5378	0.7652	6.10	4.8	0.662683	0.270539
0.24	23.56	2.5364	0.7648	4.79	5.0	0.662336	0.270398
0.32	19.02	2.5233	0.7608	5.91	7.6	0.658872	0.268983
0.40	17.01	2.5164	0.7587	6.59	9.0	0.657053	0.268241

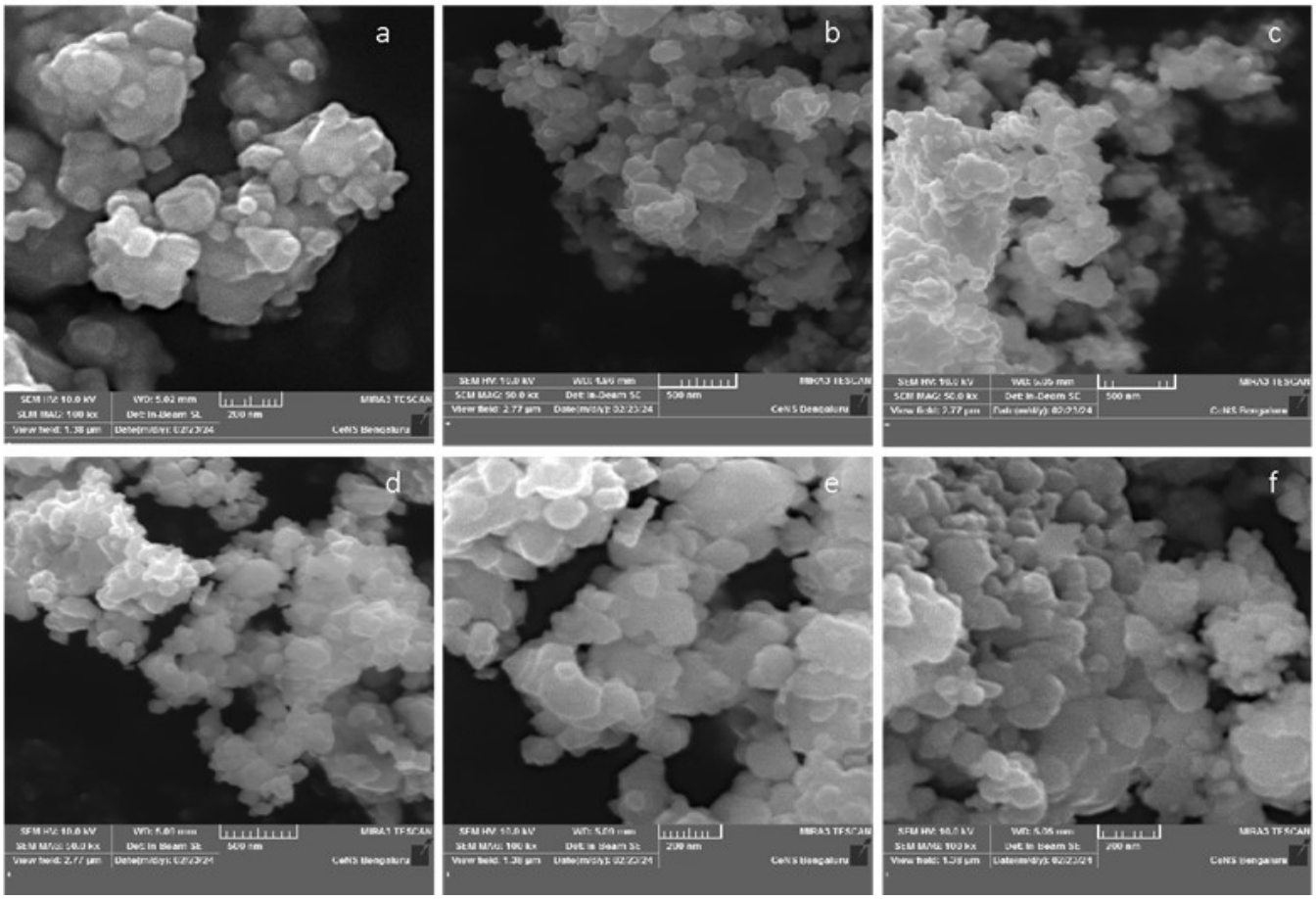

Fig. 3. FESEM image of $Co_{0.6}Zn_{0.4-x}Mg_xFe_2O_4$ samples (x = 0.00, 0.08, 0.16, 0.24, 0.32, 0.40)

Mg, Fe and O. Since the compositions match the percentages of atomic weight, no indications of impurities are observed. Table-2 lists the compositional atomic percentages of Co^{2+}, Zn^{2+}, Fe^{3+} and Mg^{2+} ions as determined by EDAX in the ferrite samples. The elemental mapping images produced by EDX analysis are shown in Fig. 5. Cobalt, zinc, magnesium and iron all show close matches in their distribution, suggesting that these metals colocalize. These finding suggests that $Co_{0.6}Zn_{0.4-x}Mg_xFe_2O_4$ nanoparticles are uniformly distributed across the studied region because of the persistent particle presence there. Moreover, the homogeneous morphology of the composite is consistent with the mapping of iron, zinc, magnesium and cobalt.

TABLE-2
EDAX DATA OF THE ATOMIC PERCENTAGES OF THE ELEMENTS IN $Co_{0.6}Zn_{0.4x}Mg_xFe_2O_4$ SAMPLES

Composition	Co^{2+}	Zn^{2+}	Fe^{2+}	Mg^{2+}
0.00	21.10	12.10	66.00	0
0.08	21.51	9.44	66.06	2.99
0.16	22.31	7.10	65.19	5.40
0.24	24.46	3.99	64.13	7.41
0.32	19.69	1.87	66.81	11.63
0.40	21.01	0.15	68.08	10.76

Electrical properties

Dielectric constant: Electric dipoles can change their polarization orientation in reaction to an applied electric field, which causes a correlation between a dielectric constant (ε′) and the polarizability of its dipole moments. According to Verwey & Boer's proposal, the electrons are transferred within ions of the same element that have different valence states and are dispersed randomly on analogous locations within the lattice to form ferrites. The electronic transition from Fe^{3+} to Fe^{2+} ions, which is crucial for conduction in ferrites, is also brought about by this electron exchange.

At room temperature, the dielectric dispersion of the samples was examined in the frequency range of 100 Hz to 5 MHz. The actual dielectric constant (ε_0) of the synthesized Mg-doped Co-Zn ferrite nanoparticles was plotted against the applied frequency. The interfacial polarization response of the dielectric dispersion exhibited the typical Maxwell-Wagner type, wherein it decreased as the applied field frequency increased. The diele-ctric constant either neared saturation or had an almost frequency independent response after declining significantly up to 5 KHz as observed from the graph [23]. The following formulae were used to compute the dielectric constant (ε′), dielectric loss factor (ε″) and AC conductivity (σ_{ac}):

$$\varepsilon' = \frac{Cd}{\varepsilon_o A}$$

$$\varepsilon'' = \varepsilon' \tan \delta$$

$$\sigma = 2\pi f \varepsilon' \varepsilon_o \tan \delta$$

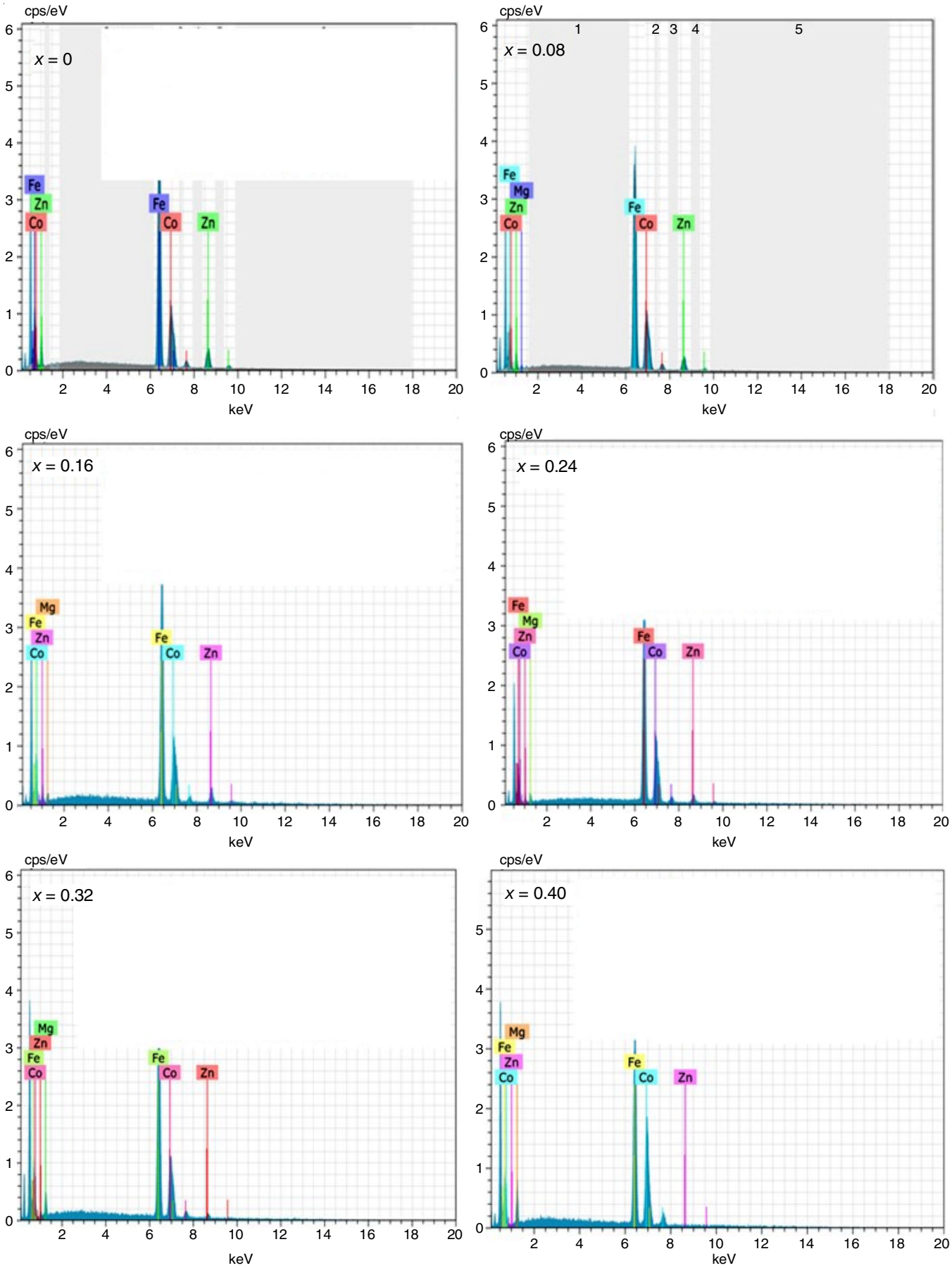

Fig. 4. EDX spectra of $Co_{0.6}Zn_{0.4-x}Mg_xFe_2O_4$ samples (x = 0.00, 0.08, 0.16, 0.24, 0.32, 0.40)

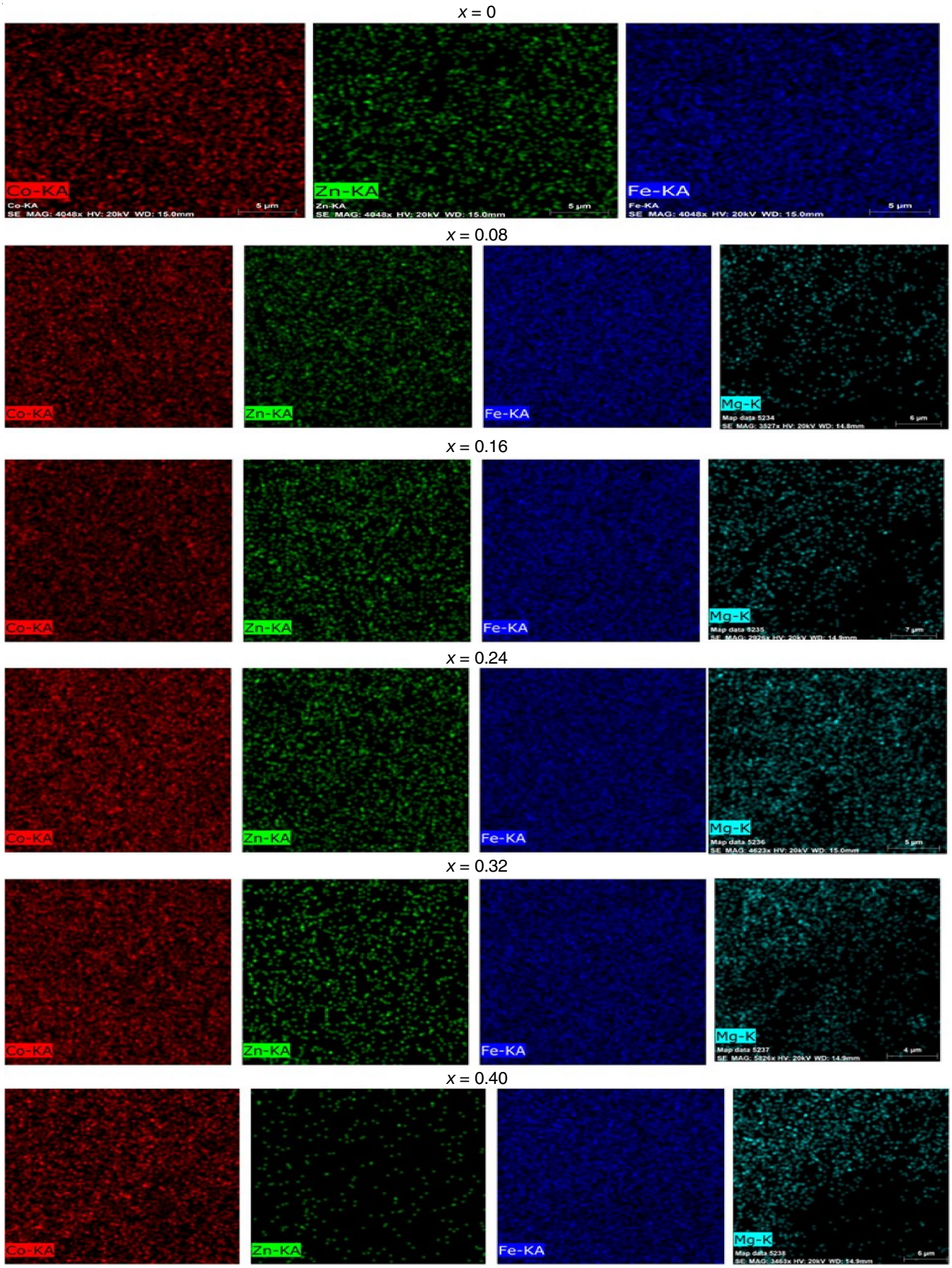

Fig. 5. Mapping images of $Co_{0.6}Zn_{0.4-x}Mg_xFe_2O_4$ for visualizing elements arrangement

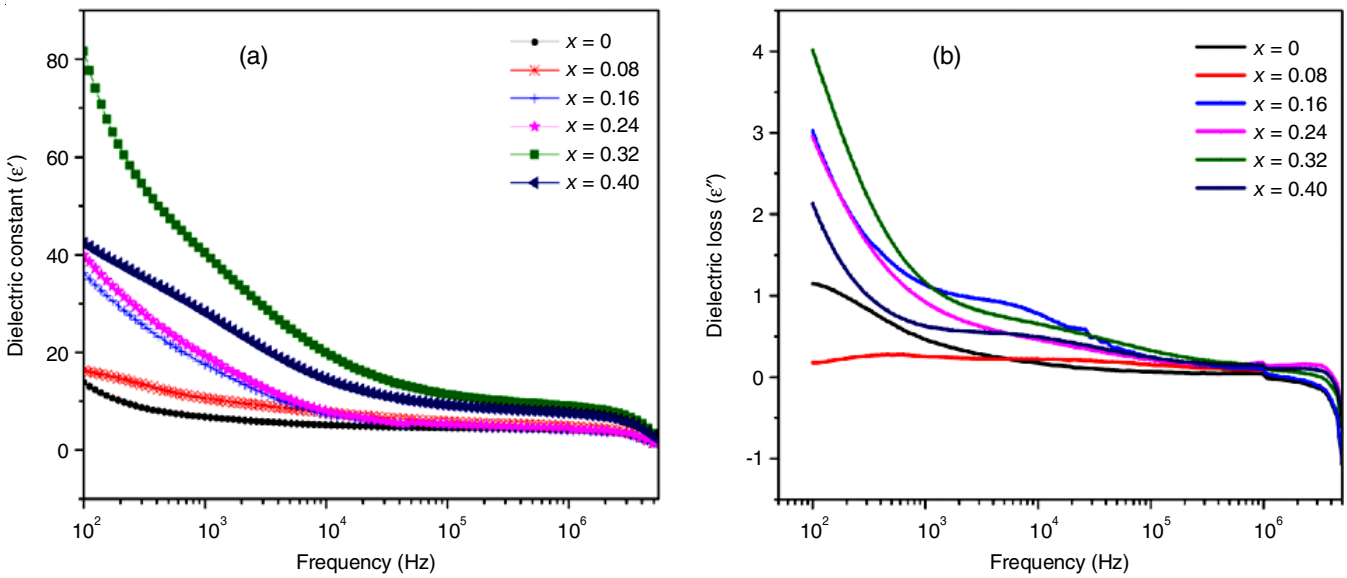

Fig. 6. Variation in frequency with respect to the (a) dielectric constant and (b) dielectric loss of $Co_{0.6}Zn_{0.4-x}Mg_xFe_2O_4$ (x = 0.00, 0.08, 0.16, 0.24, 0.32, 0.40) at room temperature

where C is the capacitance of pellet in Farad; d is the thickness of pellet in meters; A is the cross-sectional area of pellet; f is the frequency in Hz and ε_o is the permittivity of free space (8.85×10^{-12} F m^{-1}) [24].

The grain size, porosity, cation distribution, chemical composition and fabrication technique are some of the variables that affect the dielectric characteristics of the ferrite materials. Fig. 6 shows the variation in the dielectric constant as a function of frequency at room temperature. All the prepared samples have a high dielectric constant at low frequencies, which diminishes with increasing frequency and ultimately reaches a minimum at high frequencies, consistent with the typical behaviour of ferrite materials and the similar results are also observed in the literature [24-26].

The dielectric loss and dielectric constant decreased with the increasing frequency. The dielectric loss and constant decreased drastically as the frequency changed from low to high and both permittivity components were no longer frequency dependent. This behaviour was described by Koop's model and based on this model, the spinel ferrites were composed of well-conducting grains divided by extremely resistive borders [18,27].

AC conductivity: Investigation on the AC conductivity of Mg-substituted Co-Zn ferrites generally examines the impact of Mg ion incorporation on the electrical characteristics of the ferrite material. This includes examining parameters such as the frequency dependence of conductivity, the activation energy of conduction and the influence of Mg content on conductivity behaviour.

The conductivity (σ) grows with temperature, suggesting a thermally stimulated conduction process. Interestingly, there are two different behaviours that the conductivity displays that depend on the frequency: (i) For a given temperature, the conductivity is constant at low frequencies up to around 1000 Hz, indicating a homogenous conductance that is attributed to the direct current conductivity (σ_{dc}); (ii) the conductivity exhibits an increase at higher frequencies, indicating an extra charge carrier inflow and improved carrier hopping processes between successive locations in the material. The dispersion behaviour associated with these phenomena is called AC conductivity (σ_{ac}).

Fig. 7 depicts the variation in the frequency of room temperature alternating the current electrical conductivity and found that the frequency and AC electrical conductivity both increase. The conduction in ferrites is caused by electron hopping between the Fe^{2+} and Fe^{3+} ions at nearby octahedral sites [28]. The Maxwell-Wanger double layer model has been utilized to explain the frequency dependence. The high conductivity grains are produced in the samples by the ferrous ions that occur when the ferrite powder is sintered under somewhat decreasing conditions. Such materials can create low-conductivity layers when cooled in an oxygen atmosphere [29]. Ferrites displaying the non-uniform dielectric characteristics result from their enhanced conductivity layers. Grain borders and the grain itself have distinct characteristics, since these grain boundaries are more

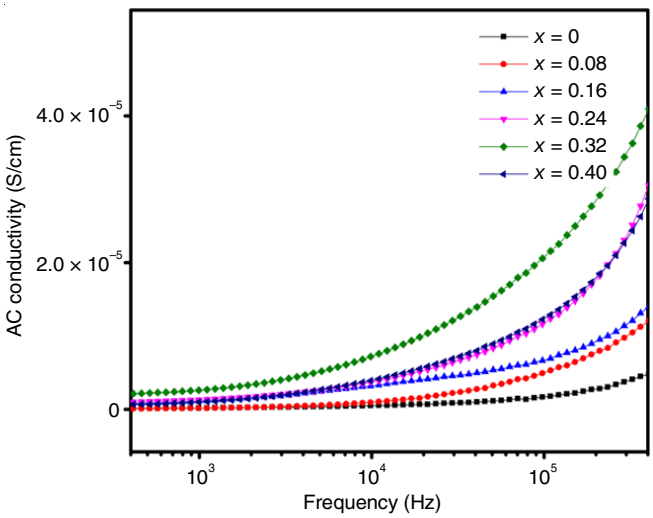

Fig. 7. Variation in AC conductivity with frequency at room temperature

active at lower frequencies, less electron hopping occurs between the Fe^{2+} and Fe^{3+} ions. By promoting the hopping of electrons between Fe^{2+} and Fe^{3+} ions, the conductive grains exhibited heightened activity as the frequency escalated, so boosting the rate of hopping. Consequently, as frequency increases, the AC electrical conductivity also increases [30].

Conclusion

The sol-gel auto-combustion was used to synthesize Mg-substituted cobalt-Zn ferrite nanoparticles with the formula $Co_{0.6}Zn_{0.4-x}Mg_xFe_2O_4$ (x = 0.00, 0.08, 0.16, 0.24, 0.32, 0.40). The FESEM images showed the well-distributed, fine-grained, spherically shaped particles. Partial agglomerations exhibit the continuous grain expansion during sintering and strong contact between the particles. A single-phase cubic spinel structure was confirmed by FTIR analysis and X-ray diffraction. With an increasing Mg content, the lattice constant of magnesium-cobalt ferrite increases. The Debye-Scherrer's equation indicates that the typical crystallite size is between 17.01 and 27.13 nm. It is evident that when the Mg content increases, the high-frequency absorption band shifts to a lower frequency. The SEM revealed that the prepared ferrite nanoparticles had spherical, cubic particle shapes. Additionally, the prepared particles have small grains and are consistent in size. The produced samples had particle sizes between 9.80 nm and 24.92 nm. An AC conductivity study of Mg-substituted Co-Zn ferrites revealed several important insights into the electrical behaviour of these materials. Moreover, the AC conductivity behaviour demonstrates the potential applications of Mg-substituted Co-Zn ferrites in various electronic devices, such as inductors, transformers and microwave devices, where controlled electrical conductivity is crucial.

CONFLICT OF INTEREST

The authors declare that there is no conflict of interests regarding the publication of this article.

REFERENCES

1. S.F. Shaikh, M. Ubaidullah, R.S. Mane and A.M. Al-Enizi, Types, Synthesis Methods and Applications of Ferrites, In: Spinel Ferrite Nanostructures for Energy Storage Devices, Elsevier, pp. 51-82 (2020).
2. A. Faraz and N.M. Ahmad, *Adv. Appl. Ceramics*, **111**, 381 (2012); https://doi.org/10.1179/1743676112Y.0000000013
3. A. Goldman, Handbook of Modern Ferromagnetic Materials, Kluwer Academic Publishers, Boston, USA (1999).
4. S. Gautam, R. Charak, S. Garg, N. Goyal, S. Chakraverty, K.H. Chae and Y. Kim, *J. Magn. Magn. Mater.*, **593**, 171867 (2024); https://doi.org/10.1016/j.jmmm.2024.171867
5. A. Vedrtnam, K. Kalauni, S. Dubey and A. Kumar, *AIMS Mater. Sci.*, 7, 800 (2020); https://doi.org/10.3934/matersci.2020.6.800
6. T. Dippong, F. Goga, E.-A. Levei and O. Cadar, *J. Solid State Chem.*, **275**, 159 (2019); https://doi.org/10.1016/j.jssc.2019.04.011
7. D.Q. Han, D.H. Yin, J. Ma, F. Wang and C.L. Li, *Ceram. Int.*, **44**, 22997 (2018); https://doi.org/10.1016/j.ceramint.2018.09.099
8. M.A. Almessiere, Y. Slimani, S. Guner, M. Sertkol, A. Demir Korkmaz, S.E. Shirsath and A. Baykal, *Ultrason. Sonochem.*, **58**, 104654 (2019); https://doi.org/10.1016/j.ultsonch.2019.104654
9. R. Qindeel and N.H. Alonizan, *Curr. Appl. Phys.*, **18**, 519 (2018); https://doi.org/10.1016/j.cap.2018.03.004
10. I.J.C. Lynda, M. Durka, A. Dinesh, A. Manikandan, S.K. Jaganathan, A. Baykal and S.A. Antony, *J. Supercond. Nov. Magn.*, **31**, 3637 (2018); https://doi.org/10.1007/s10948-018-4623-x
11. S. Asiri, M. Sertkol, S. Guner, H. Gungunes, K.M. Batoo, T.A. Saleh, H. Sozeri, M.A. Almessiere, A. Manikandan and A. Baykal, *Ceram. Int.*, **44**, 5751 (2018); https://doi.org/10.1016/j.ceramint.2017.12.233
12. A. Silambarasu, A. Manikandan and K. Balakrishnan, *J. Supercond. Nov. Magn.*, **30**, 2631 (2017); https://doi.org/10.1007/s10948-017-4061-1
13. G. Padmapriya, A. Manikandan, V. Krishnasamy, S.K. Jaganathan and S.A. Antony, *J. Supercond. Nov. Magn.*, **29**, 2141 (2016); https://doi.org/10.1007/s10948-016-3527-x
14. A.A. Ati, A.H. Abdalsalam and A.S. Hasan, *J. Mater. Sci. Mater. Electron.*, **32**, 3019 (2021); https://doi.org/10.1007/s10854-020-05053-4
15. L. Sun, R. Zhang, Q. Ni, E. Cao, W. Hao, Y. Zhang and L. Ju, *Physica B*, **545**, 4 (2018); https://doi.org/10.1016/j.physb.2018.05.030
16. X. Zhao, A. Sun, W. Zhang, L. Yu, Z. Zuo, N. Suo, X. Pan and Y. Han, *Mod. Phys. Lett. B*, **34**, 2050041 (2020); https://doi.org/10.1142/S0217984920500414
17. D. Chahar, P. Thakur, A.-C.A. Sun and A. Thakur, *J. Mater. Sci. Mater. Electron.*, **34**, 901 (2023); https://doi.org/10.1007/s10854-023-10273-5
18. B. Hasanain, *Mater. Res. Express*, **10**, 045004 (2023); https://doi.org/10.1088/2053-1591/acca6b
19. S. Hasan and B. Azhdar, *J. Phys. Condens. Matter*, **35**, 425303 (2023); https://doi.org/10.1088/1361-648X/ace6ed
20. B. Ingale, D. Nadargi, J. Nadargi, R. Suryawanshi, H. Shaikh, M.A. Alam, M.S. Tamboli and S.S. Suryavanshi, *ACS Omega*, **8**, 30508 (2023); https://doi.org/10.1021/acsomega.3c03757
21. H.M.H. Zakaly, S.A.M. Issa, H.A. Saudi, G.A. Alharshan, M.A.M. Uosif and A.M.A. Henaish, *Sci. Rep.*, **12**, 15495 (2022); https://doi.org/10.1038/s41598-022-17311-y
22. K.I. Hadjiivanov, D.A. Panayotov, M.Y. Mihaylov, E.Z. Ivanova, K.K. Chakarova, S.M. Andonova and N.L. Drenchev, *Chem. Rev.*, **121**, 1286 (2021); https://doi.org/10.1021/acs.chemrev.0c00487
23. M. Hadi, K.M. Batoo, A. Chauhan, O.M. Aldossary, R. Verma and Y. Yang, *Magnetochemistry*, **7**, 53 (2021); https://doi.org/10.3390/magnetochemistry7040053
24. K.E. Rady, A.R.A. El-Salam, E.A. ELFadaly and M.H. Aly, *Appl. Phys., A Mater. Sci. Process.*, **129**, 245 (2023); https://doi.org/10.1007/s00339-023-06528-x
25. M. Das, M.N.I. Khan, M.A. Matin and M.M. Uddin, *J. Supercond. Nov. Magn.*, **32**, 3569 (2019); https://doi.org/10.1007/s10948-019-5104-6
26. S. Ramesh, B. Dhanalakshmi, B.C. Sekhar, P.S.V.S. Rao and B.P. Rao, *Ceram. Int.*, **42**, 9591 (2016); https://doi.org/10.1016/j.ceramint.2016.03.043
27. K. Hussain, N. Amin and M.I. Arshad, *Ceram. Int.*, **47**, 3401 (2021); https://doi.org/10.1016/j.ceramint.2020.09.185
28. S.S. Bellad, S.C. Watawe and B.K. Chougule, *Mater. Res. Bull.*, **34**, 1099 (1999); https://doi.org/10.1016/S0025-5408(99)00107-5
29. E. Melagiriyappa, H.S. Jayanna and B.K. Chougule, *Mater. Chem. Phys.*, **112**, 68 (2008); https://doi.org/10.1016/j.matchemphys.2008.05.014
30. H.-I. Hsiang, C.-S. Hsi, C.-Y. Tsai and L.-T. Mei, *Ceram. Int.*, **41**, 4140 (2015); https://doi.org/10.1016/j.ceramint.2014.11.110